Applied Catalysis B: Environmental 89 (2009) 375–382

Contents lists available at ScienceDirect

Applied Catalysis B: Environmental

journal homepage: www.elsevier.com/locate/apcatb

Preparation, characterization and catalytic properties of carbon nanofiber-supported Pt, Pd, Ru monometallic particles in aqueous-phase reactions

Carmen Diaz Taboada [a], Jurka Batista [b], Albin Pintar [b,c,*], Janez Levec [b,c]

[a] Department of Chemical Engineering, Complutense University, Avda. Complutense s/n, ES-28040 Madrid, Spain
[b] Laboratory for Catalysis and Chemical Reaction Engineering, National Institute of Chemistry, Hajdrihova 19, P.O. Box 660, SI-1001 Ljubljana, Slovenia
[c] Department of Chemical Engineering, University of Ljubljana, Aškerčeva 5, P.O. Box 537, SI-1001 Ljubljana, Slovenia

ARTICLE INFO

Article history:
Received 29 October 2008
Received in revised form 11 December 2008
Accepted 14 December 2008
Available online 25 December 2008

Keywords:
Carbon nanofibers
Noble metal catalysts
Characterization
Catalytic wet-air oxidation
Liquid-phase thermal decarboxylation
Heterogeneous catalysis
Trickle-bed reactor

ABSTRACT

Carbon nanofibers (CNF) synthesized by catalytic chemical vapor deposition (CVD) method were used to prepare supported platinum, palladium and ruthenium monometallic (2.0 wt.%) catalysts by means of incipient-wetness impregnation method. The CNF support and catalysts were characterized by X-ray powder diffraction (XRD), nitrogen adsorption/desorption isotherms, volumetric chemisorption of hydrogen, temperature-programmed reduction (H_2-TPR) and scanning electron microscopy (SEM). Solids were tested in catalytic wet-air oxidation (CWAO) of phenol aqueous solution (180–240 °C and 10.0 bar of oxygen partial pressure) carried out in a continuous-flow trickle-bed reactor. Trends of phenol and total organic carbon (TOC) conversion demonstrate that the CNF support and CNF-Pt catalyst did not exhibit constant activity for CWAO of phenol. A decrease of catalyst activity, detection of carbon dioxide in the off-gas stream while examining catalyst stability and significant textural changes observed, provide an evidence that under net oxidizing reaction conditions gasification of the CNF support occurs. The prepared catalysts were also tested in liquid-phase thermal decarboxylation of formic acid in inert atmosphere (60–220 °C). Among solids examined, the CNF-Pd exhibited the highest activity. At the employed conditions, no decomposition of the CNF support was observed during the thermal decarboxylation of formic acid.

1. Introduction

Catalytic wet-air oxidation (CWAO) represents a promising technique for removal of toxic and non-biodegradable organic compounds from industrial wastewaters [1]. In the three-phase CWAO process, the organic pollutants are oxidized by activated O_2 species in the presence of a solid catalyst, usually at temperatures of 130–250 °C and pressures of 10–50 bar, into biodegradable intermediate products (such as low molecular weight carboxylic acids) or mineralized into CO_2, water and associated inorganic salts. The CWAO of a variety of organic pollutants has been studied over supported noble metal catalysts, metal oxides, mixed metal oxide systems and cerium-based composite oxides [2]. Several studies regarding CWAO of various organics have been performed in the presence of activated carbon or carbon-based catalysts [3,4].

Carbon materials as activated carbon, carbon nanotubes (CNT) and carbon nanofibers (CNF) are used as catalyst carriers [5]. Carbon nanotubes are materials with special carbon nanostructures (i.e. multi- or single-walled), electronic and mechanical properties, which are promising for many technological applications including energy storage, electronics and heterogeneous catalysis [6–13]. The noble metal nanoparticles (including Pd, Pt, Ru and Rh) have been applied on CNT support and examined in selective hydrogenation reactions [11,14,15]. The main advantages of carbon nanofibers compared to activated carbon are the high purity of the material, high mechanical strength, the mesoporous nature (resulting in low internal mass-transfer resistances), which makes them interesting to promote a variety of liquid-phase reactions, such as methanol oxidation, cinnamaldehyde hydrogenation and cyclohexanol dehydrogenation [11]. Furthermore, specific metal–support interactions exist in CNF-based solids that can directly affect the catalytic activity and the selectivity. As the synthesis and consequently surface properties of activated carbons are difficult to control (one should also note diffusional problems due to inappropriate textural properties), CNF could replace their use.

* Corresponding author at: Laboratory for Catalysis and Chemical Reaction Engineering, National Institute of Chemistry, Hajdrihova 19, P.O. Box 660, SI-1001 Ljubljana, Slovenia. Tel.: +386 1 47 60 283; fax: +386 1 47 60 300.
E-mail address: albin.pintar@ki.si (A. Pintar).

0926-3373/$ – see front matter © 2008 Elsevier B.V. All rights reserved.
doi:10.1016/j.apcatb.2008.12.016

Recently, platinum catalysts (1.0 wt.%) supported on multi-walled carbon nanotubes (Pt-MWCNT) were tested for catalytic wet-air oxidation of aqueous model solutions of aniline and different azo dyes and real wastewater from a textile plant [16]. It was found that Pt-MWCNT catalysts yielded complete conversion of aniline at conditions of 200 °C, 6.9 bar of oxygen and residence time of 120 min. Further, they observed that the most active Pt-CMWNT catalyst could be efficiently used for removal of azo dyes from aqueous model solutions and for improvement of total organic carbon (TOC) and color removal from wastewater resulting from a textile plant. Different support surface chemistry as well as the preparation parameters of catalysts affect the catalytic performances of MWCNT-supported metal catalysts (i.e. Cu, Pt, Ru) [16–19].

Even though there are number of reports on CNF/CNT in catalysis, none of the studies have targeted noble metal catalysts for the elimination of phenol and formic acid from model aqueous solutions or industrial wastewaters. The present work aims to get insight into the (potential) application of CNF-Pt, CNF-Pd and CNF-Ru catalysts for CWAO of phenol and thermal decarboxylation of formic acid. For this purpose, monometallic Pt, Pd and Ru nanoparticles (2.0 wt.%) were supported over synthesized carbon nanofibers. Catalytic tests were carried out in O_2 rich and He environments in a continuous-flow trickle-bed reactor, which is of the same type as the one previously packed with Ru(x wt.%)/TiO_2 catalysts (x = 1.5 and 3.0) and used for CWAO of aliphatic and aromatic model compounds [20]. Results of catalytic runs are discussed along with catalyst characterization by X-ray powder diffraction (XRD), BET, N_2 adsorption/desorption, static H_2 chemisorption, TPR and scanning electron microscopy (SEM). Catalytic performances of CNF-supported monometallic Pt, Pd and Ru materials are compared to those observed over conventional Ru/TiO_2 catalysts under similar operating conditions.

2. Experimental

2.1. Synthesis and purification of CNF support

The high quality carbon nanofibers were synthesized by catalytic chemical vapor deposition (CVD) method using γ-alumina-supported iron as catalyst and acetylene as carbon source in a tubular quartz reactor. The raw CNF produced in the CVD step was then purified by a hydrofluoric acid treatment to remove the residual catalyst particles and carbonaceous impurities.

The Fe(20 wt.%)/γ-Al_2O_3 catalyst used in the CVD step was prepared by incipient-wetness impregnation of γ-Al_2O_3 support with an aqueous solution of $Fe(NO_3)_3{\cdot}9H_2O$ (99.0 wt.%, Merck), followed by drying (100 °C) and calcination (in air at 450 °C for 2 h). The calcined catalyst precursor (0.20 g in a quartz crucible) was placed in a quartz tubular reactor (horizontal furnace and a quartz tube with a diameter of 0.08 m and a length of 1.2 m), purged (30 min at room temperature) in H_2/N_2 (2:1) flow (100 ml/min) and reduced at 650 °C for 2 h. The hydrogen flow was then stopped and replaced by acetylene (99.9% purity, Messer) flow (40 ml/min), while the temperature was increased (20 °C/min) up to 700 °C. The synthesis of CNF was continued for 1 h at the same temperature. The raw CNF product was suspended in 48% HF and vigorously stirred at room temperature for 15 h to eliminate impurities. The obtained material was filtered, washed several times with distilled water and dried at 110 °C for 24 h.

2.2. Catalyst preparation

CNF-Pt, CNF-Pd and CNF-Ru catalysts were prepared by incipient-wetness impregnation of CNF carrier with an aqueous solution of metal precursors $H_2PtCl_6{\cdot}6H_2O$ (99.99 wt.%, Aldrich), Na_2PdCl_4 (98 wt.%, Aldrich), and $RuCl_3{\cdot}xH_2O$ (35–40 wt.% Ru, Acros Organics), respectively. The concentrations of the metal precursors in the impregnating solutions were calculated in order to prepare catalysts with a nominal metal loading of 2.0 wt.%. The excess water was then removed in a rotary evaporator and the impregnated materials were dried in air overnight at 110 °C. The dried catalyst precursors were reduced in hydrogen flow of 250 ml/min (CNF-Pt and CNF-Pd: 1 h at 150 °C; CNF-Ru: 1 h at 200 °C) at a heating rate of 3 °C/min. The reduced samples were cooled down to room temperature under inert N_2 flow. Reduction conditions were determined in this work by TPR analysis of dried catalyst precursors.

Table 1
Specific surface area (S_{BET}), total pore volume (V_{pore}), average pore width (d_{pore}) and metal dispersion (D) of fresh CNF-Pt, CNF-Pd and CNF-Ru catalysts prepared by incipient-wetness impregnation method and reduced directly in H_2 flow.

Sample	S_{BET} (m^2/g)	V_{pore} (cm^3/g)	d_{pore} (nm)	D[a] (%)
CNF	215	1.16	22	–
CNF-Pt	207	1.07	21	26
CNF-Pd	192	0.99	21	6.1
CNF-Ru	203	1.07	21	6.5

[a] Hemispherical shape of metal particles and M:H = 1:1 stoichiometry was assumed in calculations of metal dispersion.

2.3. Catalyst characterization

The specific BET surface area, total pore volume and average pore width of catalysts were determined from the adsorption and desorption isotherms of N_2 at −196 °C using a Micromeritics ASAP 2020 MP/C instrument. This characterization was carried out after degassing of samples to 4 μm Hg for 1 h at 90 °C and 2 h at 300 °C. The same apparatus was used to perform static H_2 chemisorption analyses (T = 35 °C for CNF-Pt and CNF-Ru; T = 90 °C for CNF-Pd, which is well above the temperature of Pd hydride decomposition). Results of physisorption and static H_2 chemisorption measurements are shown in Tables 1 and 2. Temperature-programmed reduction (H_2-TPR) measurements of samples were performed with a Micromeritics Autochem II 2920 catalyst characterization system connected to a Pfeiffer Vacuum mass spectrometer (model ThermoStar). Continuous analysis of the outlet gas stream during H_2-TPR analysis was carried out by TCD and mass spectrometer (MS) detectors. The MS signals at m/e = 2 (H_2), 15 (CH_4), 18 (H_2O), 28 and 30 (CO), 44 (CO_2), and 36 (HCl) were recorded continuously. The optimal reduction conditions for dried catalyst precursors were determined from the obtained H_2-TPR/MS results.

X-ray powder diffraction patterns of the support as well as fresh and used catalyst samples (Fig. 1) were obtained on a PANalytical X'Pert PRO diffractometer using Cu Kα radiation (λ = 0.15406 nm). Data were collected from 20 to 90° 2θ, at 0.034° and 100 s per step. Crystalline phases were identified by comparison with the reference data from ICDD (International Centre for Diffraction Data) files.

The high resolution scanning electron micrographs of fresh and spent catalyst samples were recorded on a FE-SEM SUPRA 35VP (Carl Zeiss) microscope equipped with an EDAX energy dispersive X-ray spectrometer Inca 400 (Oxford Instruments).

Table 2
Textural properties and metal dispersion of catalysts used in different catalytic runs.

Sample	Model pollutant	S_{BET} (m^2/g)	V_{pore} (cm^3/g)	d_{pore} (nm)	D (%)
CNF-PhOH	Phenol	258	0.78	12	–
CNF-Pt-PhOH	Phenol	163	0.38	9	–
CNF-Pt-FA	Formic acid	202	0.97	19	23
CNF-Pd-FA	Formic acid	202	0.97	19	1.1
CNF-Ru-FA	Formic acid	215	1.07	20	3.0

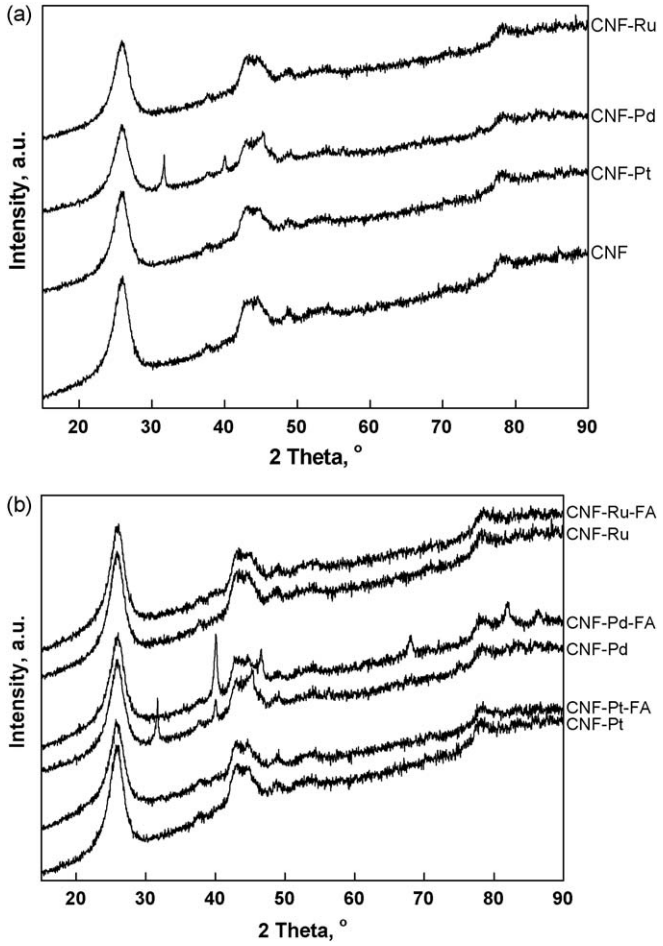

Fig. 1. X-ray powder diffraction patterns of: (a) fresh CNF-Pt, CNF-Pd and CNF-Ru catalyst samples and (b) catalysts after the treatment of formic acid (FA) in inert He atmosphere. Metal loading: 2.0 wt.%.

2.4. Catalytic runs

CWAO runs were carried out in the Microactivity-Reference unit (PID Eng&Tech, model MA-Ref), which is an automated and computer-controlled continuous-flow trickle-bed laboratory reactor. The catalytic reactor and operating conditions are described in detail in Ref. [20]. The reactor operated in the low-interaction (LIR) trickle-flow regime at T = 60–240 °C and $P_{tot.}$ = 10–44 bar (oxygen partial pressure was in the range of 0.0–10.0 bar). Concentrations of the initial aqueous solutions were 2.0 g/l for formic acid (100%, Merck) and 1.0 g/l for phenol (99%, Aldrich). The fixed-bed tubular reactor (Hastelloy C-276 tube, 20 ml i.v., 9 mm i.d., Autoclave Engineers) was heated with a reactor furnace and integrated within the hot box. The liquid reactant was introduced at a flow rate of 1.0 ml/min (superficial liquid flow rate equals to 0.27 kg/m^{2}s) into the unit using a HPLC positive alternative displacement pump (Gilson, model 307). The preheated gas stream (superficial gas flow rate was in the range of 0.33–0.93 kg/m^{2}s) and liquid stream merge and are then introduced to the top of the reactor. A Hastelloy C-276 porous (2 μm) plate placed inside near the middle of the reactor tube supported the fixed bed composed of about 0.45–0.50 g of either CNF support or catalyst. The reaction temperature was regulated within the limits ±1.0 °C (K-thermocouple; PID temperature controller TOHO, model TTM-005). The gas- and liquid-phase, which flowed out at the bottom of the bed, were separated in a liquid–gas separator cooled with a Peltier cell. In the off-gas stream, production of carbon dioxide and eventual production of carbon monoxide were monitored by a non-dispersive infrared detector (Rosemount, model BINOS 1001).

2.5. Wet-air oxidation (WAO) reaction conditions effect

To analyze an influence of WAO conditions on the modification of bare CNF support and catalysts (CNF-Pt, CNF-Pd, CNF-Ru), additional experiments were performed at $p(O_2)$ = 10.0 bar by using distilled water (pH = 5.5) at a flow rate of 1.0 ml/min in the temperature range from 100 to 240 °C. After each time on stream, TOC value in the liquid-phase and CO_2 content in the gas-phase were determined.

2.6. Analysis of end-product solutions (HPLC, TOC)

The reaction products were analyzed by HPLC (HP, model 1100) equipped with a 250 mm × 4.6 mm Synergi 4μ Hydro-RP column or with a 150 mm × 4.6 mm Spherisorb ODS2 5μ column for identification and quantification of organic acids and phenol, respectively. Analytical details are given in Ref. [20]. The total amount of organic substances in aqueous-phase samples was determined by measuring the total organic carbon. TOC was determined with a Rosemount/Dohrmann DC-190 TOC analyzer, by subtracting measured inorganic carbon (IC) content from measured total carbon (TC) content.

3. Results and discussion

3.1. Catalyst characterization

In Fig. 1a the effect of platinum, palladium and ruthenium loading on phase formation during the preparation of CNF-Pt, CNF-Pd and CNF-Ru catalysts is shown. The XRD pattern of synthesized CNF support is also included for comparison. X-ray diffraction analysis reveals the graphitized nature of carbon in the CNF support that is confirmed by the presence of C (0 0 2) and C (1 0 0) reflections at 2θ close to 26 and 42.8° (a very broad peak), respectively. Deposition of platinum and ruthenium species on CNF support and further reduction of catalyst precursors in hydrogen atmosphere led to the formation of Pt^0 and Ru^0 phases that cannot be detected by means of the XRD technique. The broadening of diffraction peaks is too large to identify Ru nanoparticles in the CNF-Ru catalyst. The (1 0 0), (0 0 2), and (1 0 1) reflections at 2θ close to 38.4, 42.2, and 44.0°, respectively, assigned to the hexagonal structure of ruthenium (ruthenium, syn, PDF 00-006-0663) are overlapped by diffraction peaks of CNF in the regions 37–39 and 41–46° (Fig. 1a). Hence, the structural identification of Ru^0 phase is rendered. On the other hand, XRD pattern of the CNF-Pd catalyst indicates the presence of metallic palladium phase (palladium, syn, PDF 046-1043: 2θ = 40.1°) and some residual sodium chloride species (2θ close to 31.0 and 44.5°), which originate from the palladium precursor Na_2PdCl_4.

The presence of rather large and discrete metallic Pd and Ru particles and very fine Pt particles on the surface of synthesized monometallic catalysts is revealed by H_2 chemisorption measurements (18, 20 and 4 nm for CNF-Pd, CNF-Ru and CNF-Pt, respectively). The SEM micrographs (Fig. 2) clearly illustrate that the applied catalyst preparation procedure has no significant effect on the morphology and microscopic features of external CNF surface.

The textural properties of bare CNF support and catalysts were determined from nitrogen adsorption–desorption isotherms. The N_2 adsorption measurements revealed Type II isotherm for the support as well as catalyst samples [21]. The Brunauer–Emmet–Teller (BET) method was employed to calculate the BET specific surface area of all samples from their nitrogen adsorption

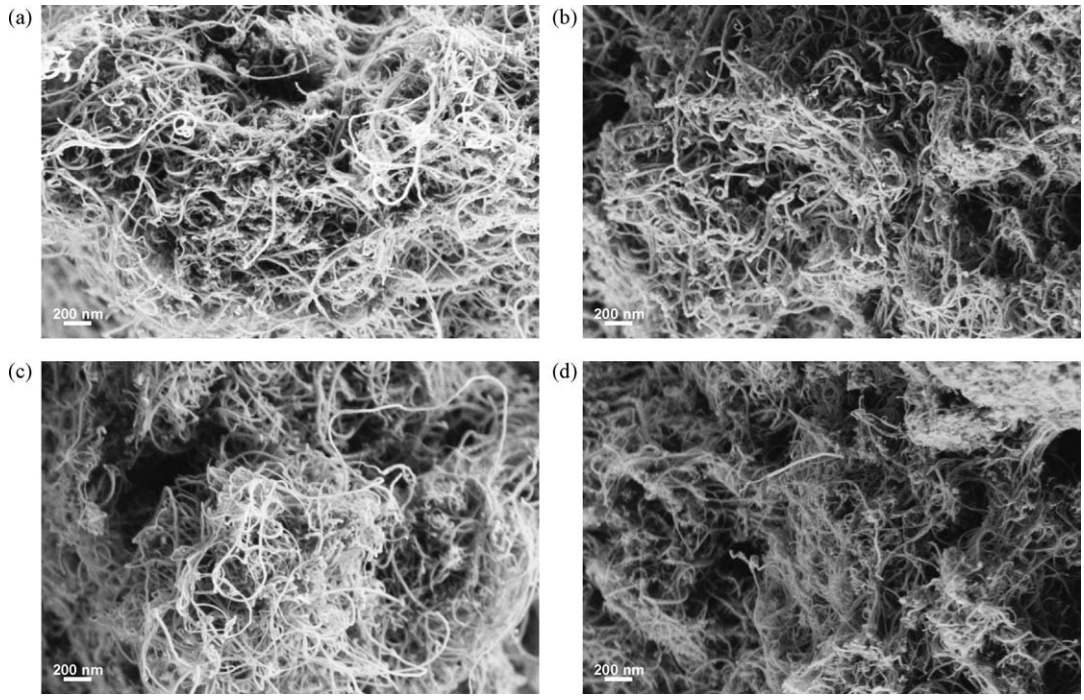

Fig. 2. SEM micrographs of fresh carbon nanofibers and carbon nanofiber-supported monometallic catalysts: (a) CNF, (b) CNF-Pt, (c) CNF-Pd and (d) CNF-Ru.

isotherms that are presented in Fig. 3. BET surface area, total pore volume (obtained from the amount of N_2 adsorbed at $p/p^\circ = 0.98$) and average pore diameter (BJH method) of catalysts (Table 1) indicate that deposition of 2.0 wt.% of metal did not markedly change the textural properties of the CNF support.

H_2-TPR profiles measured in the temperature range from −40 to 500 °C during the reduction of catalyst precursors and CNF support by means of TCD detector are shown in Fig. 4. The formation of HCl, water, methane, CO and CO_2 during H_2-TPR examinations of prepared samples was simultaneously measured by TCD detector and mass spectrometer (MS). We observed high resistance of the CNF support upon hydrogen exposition during TPR run up to 400 °C (Fig. 4, no H_2 consumption peaks). In the case of CNF-Pd precursor, a small negative peak with maximum at 55 °C (H_2 evolution) can be attributed to decomposition of Pd hydride phase formed at lower temperature, while a high temperature H_2 consumption peak (T_{max} close to 127 °C) is associated with the reduction of Pd^{2+} ions to Pd^0 [22,23]. The reduction step and the simultaneous formation of HCl and water (MS, not shown) are completed below 160 °C (Fig. 4). The H_2-TPR profiles of CNF-Pt and CNF-Ru catalyst precursors show the H_2 consumption peaks in the temperature range from 40 to 242 °C, assigned to the reduction of platinum ion species (Fig. 4, T_{max} close to 130 °C) and ruthenium ion species (two maxima close to 100 and at 175 °C) in accordance with the HCl and water formation determined by simultaneous MS analysis.

The H_2-TPR profiles of dried catalyst precursors reveal that aqueous solutions of metal precursors (H_2PtCl_6, Na_2PdCl_4 and $RuCl_3$) interacted differently with the CNF surface. In the case of CNF-Pd and CNF-Ru catalyst precursors, TPR spectra exhibit two peaks (Fig. 4). This may be ascribed to the presence of two catalyst precursor phases interacting differently with the CNF support,

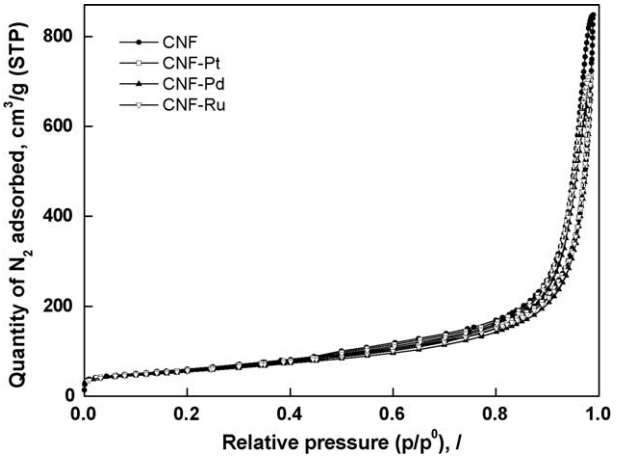

Fig. 3. N_2 adsorption–desorption isotherms of CNF support and catalyst samples measured at −196 °C.

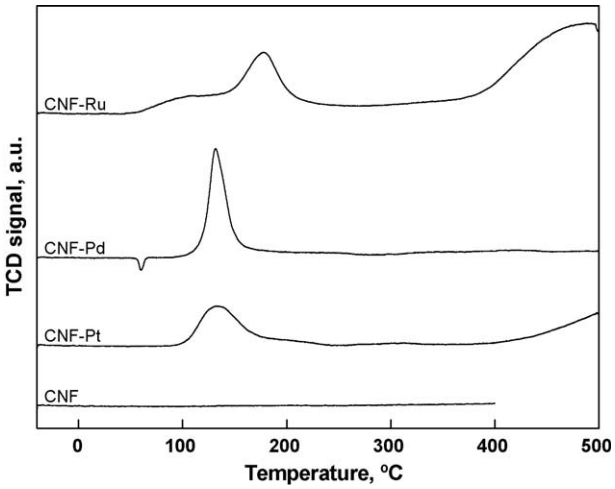

Fig. 4. H_2-TPR profiles of bare CNF support and catalysts precursors obtained in the temperature range from −40 to 500 °C. Operating conditions: 50 ml/min (STP), H_2 (5 vol.%)/Ar, 5 °C/min. Sample weight, 150 mg.

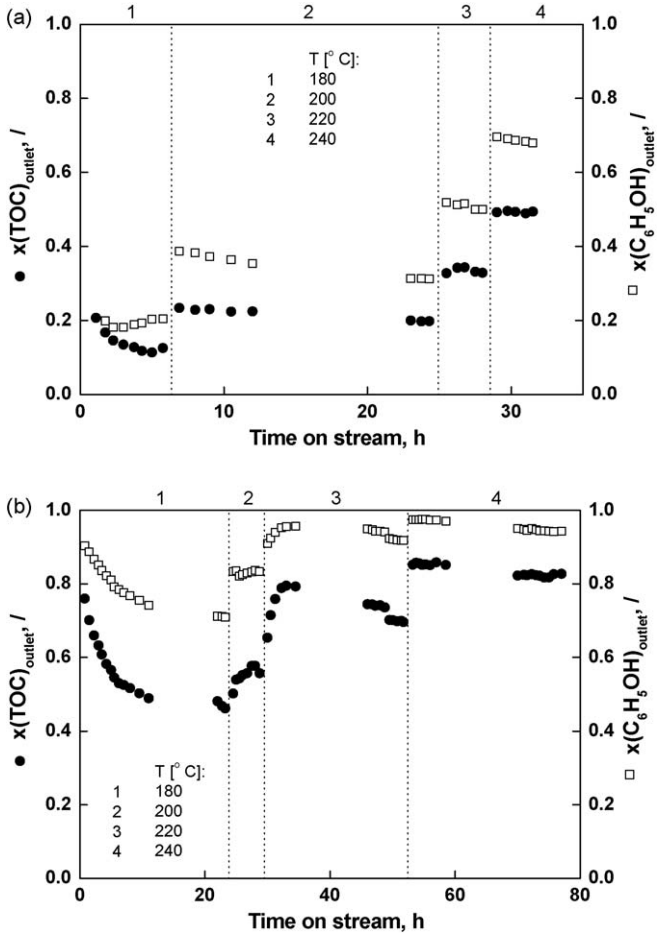

Fig. 5. Phenol and TOC conversion as a function of time on stream measured during liquid-phase phenol oxidation in a trickle-bed reactor at various reaction temperatures over: (a) bare CNF support and (b) CNF-Pt catalyst. $p(O_2)$: 10.0 bar, volumetric flow rate ($\Phi_{vol,L}$): 1.0 ml/min, phenol feed concentration ($c(C_6H_5OH)_{feed}$): 1.0 g/l. Catalyst weight, 500 mg.

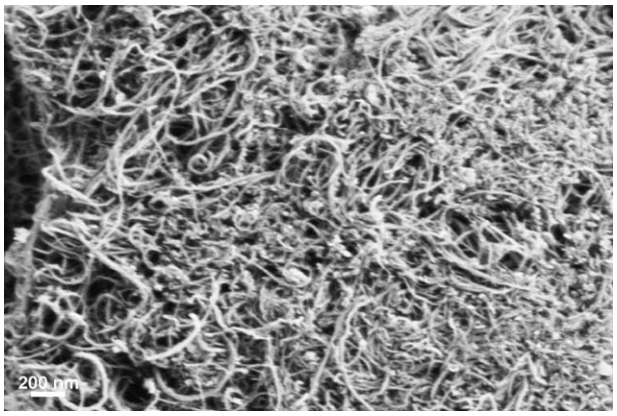

Fig. 6. SEM micrograph of bare CNF support used in CWAO of aqueous phenol solution. Reaction conditions: see Fig. 5.

which might due to weak adsorption of precursor species lead to a broad metal particle size distribution and poor dispersion. On the other hand, reduction of CNF-Pt precursor (one TPR peak) leads to the formation of smaller Pt particles, which can be attributed to stronger precursor–support interaction.

At the employed reduction treatment, H_2-TPR/MS measurements of CNF-Pt and CNF-Ru catalyst precursors evidenced that gasification of the CNF support by H_2 starts close to 350 °C (Fig. 4) and leads to the formation of methane; no formation of C2 compounds was observed. It can be noticed from Fig. 4 that reduced Pt and Ru species catalyze reaction between the CNF support and hydrogen. This reaction is more obvious in the presence of Ru^0 (CNF-Ru sample). Among the prepared catalysts, CNF-Pd sample exhibited the best thermal stability under H_2-TPR reaction conditions. It should be pointed out that methane formation was not detected up to 500 °C.

3.2. Catalytic runs

3.2.1. CWAO of phenol

Fig. 5a and b show phenol and TOC conversion as a function of time on stream in consecutive oxidation runs carried out at various reaction temperatures (180–240 °C) in the presence of bare CNF support or CNF-Pt catalyst. The support exhibited catalytic activity under oxidizing conditions ($p(O_2)$ = 10.0 bar, liquid flow rate of 1.0 ml/min, $c(\text{phenol})_{feed}$ = 1.0 g/l) at temperatures ≥180 °C (~20% TOC reduction), which is similar to the results of Yang et al. [24]. It is evident from Fig. 5a that after a longer period of operation at 180 °C, lower TOC removal in the reactor outlet was observed. Further increase in phenol and TOC conversion with time on stream in subsequent oxidative steps was observed after each increase of reaction temperature (Fig. 5a, steps 2–4). For instance, TOC conversion increases from 10% at T = 180 °C to 50% at T = 240 °C. The TOC conversion was improved above 180 °C, which is besides higher reaction temperature attributed to desorption and destruction of intermediate C-6 products (such as benzoquinones and hydroquinones) previously accumulated on the CNF surface [20]. Examination of the textural properties of support after reaction under oxidative conditions showed that bare CNF support was modified significantly (Tables 1 and 2; BET surface area: 215 and 258 m^2/g, total pore volume: 1.16 and 0.78 cm^3/g, average pore width: 22 and 12 nm for fresh and used support, respectively). Also, the appearance of the CNF support after CWAO of phenol (Fig. 6) and fresh CNF (Fig. 2a) are quite different, which is due to the presence of adsorbed reaction intermediates on the CNF surface.

A comparison of results illustrated in Fig. 5a and b shows that phenol was more easily oxidized in the presence of CNF-Pt catalyst. During the first oxidation step (T = 180 °C), a decrease in phenol and TOC conversion can be again observed with time on stream. For example, at this temperature TOC conversion decreases from the initial value of ~75 to ~45% at t = 24 h and from 20 to 10% after 5.5 h of reaction over the CNF-Pt catalyst and bare support, respectively. Simultaneously, a change of color from light yellow to dark brown in the outlet liquid-phase was observed that was accompanied with the foam formation. The decrease of TOC conversion with time on stream at constant temperature ($T \leq 200$ °C) was not only due to partial oxidation of the CNF support at this operating conditions, but also due to strong adsorption of intermediates formed during the oxidative phenol treatment. As in the case of Ru/TiO_2 catalysts [20], the color change in the outlet liquid-phase demonstrated the formation of C-6 aromatic intermediates (i.e. benzoquinones, hydroquinones), which was also confirmed by HPLC analysis. During an increase of reaction temperature ($T \geq 200$°C) in next steps (Fig. 5a and b, steps 2–4), the CNF and CNF-Pt exhibited higher phenol and TOC conversion due to considerable desorption and destruction of C-6 intermediates previously accumulated on the active surface. For instance, TOC conversion over the CNF-Pt catalyst increases from 45 to 84% with an increase of temperature from 180 to 240 °C. A comparison of phenol and TOC conversion obtained over the CNF-Pt (Fig. 5b) and Ru/TiO_2 catalysts [20], which were tested under the same reaction conditions but at different catalyst loading (i.e. 0.50

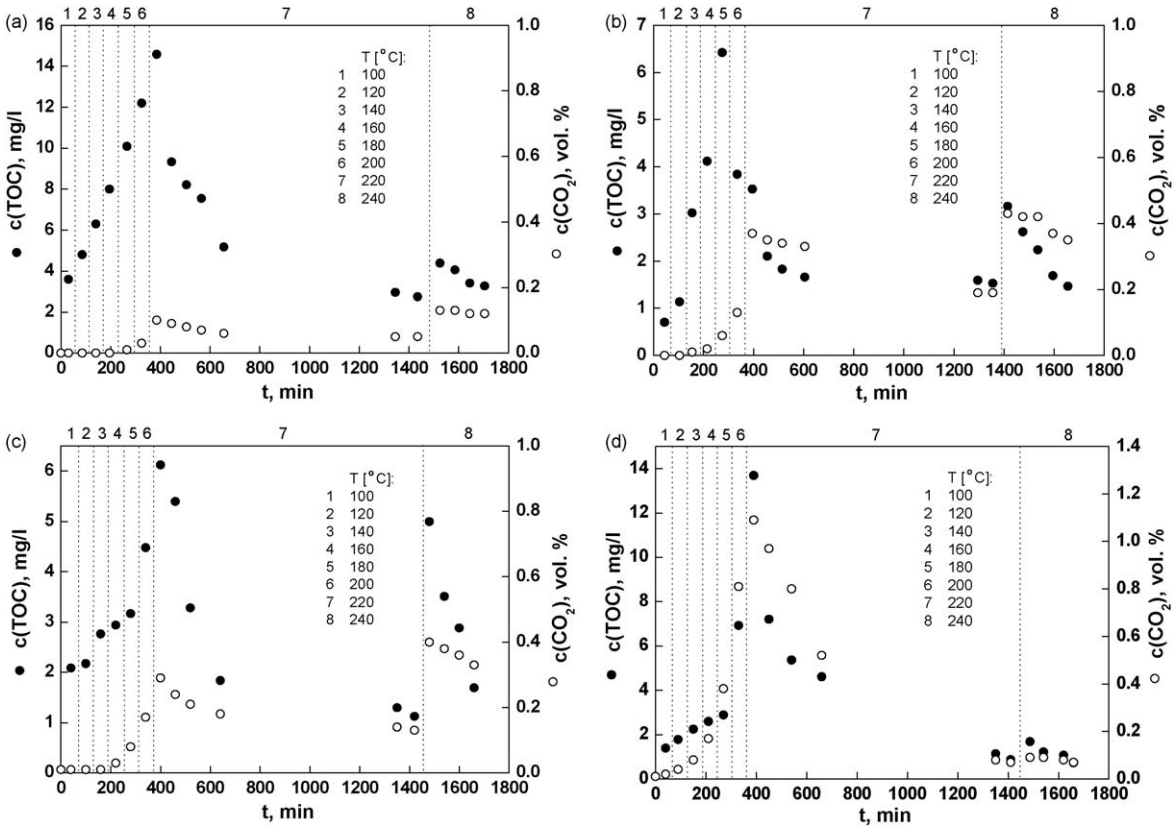

Fig. 7. TOC content in liquid-phase and CO_2 concentration in off-gas stream as a function of time on stream obtained during exposition of: (a) bare CNF support, (b) CNF-Pt, (c) CNF-Pd and (d) CNF-Ru catalysts to oxidative operating conditions in a trickle-bed reactor. $p(O_2)$: 10.0 bar, $\Phi_{vol.,L}$: 1.0 ml/min, feed solution: distilled water.

and 3.0 g for CNF-Pt and Ru/TiO_2, respectively), indicates that the CNF-Pt catalyst sample exhibits higher activity for CWAO of phenol. However, trends of phenol and TOC conversion at a given temperature demonstrate that the bare support and CNF-Pt catalyst did not exhibit constant activity for CWAO of phenol.

Activity measurements coupled with the physicochemical characterization of spent CNF support and CNF-Pt catalyst after CWAO of phenol (significant textural modifications of catalyst samples are listed in Table 2) demonstrate that higher reaction temperatures are favorable for the oxidation of phenol (in order to avoid blockage of the catalyst surface by strongly adsorbed C-6 intermediates), but clearly exhibit negative effect ($T \geq 200$°C) on long-term operation, as no steady-state operation of the reactor was obtained at any of examined temperatures, especially over the CNF-Pt catalyst (Fig. 5). Besides sintering of metal clusters, this might be attributed to partial oxidation of CNF to CO_2 and water taking place in parallel to CWAO of phenol. To confirm this hypothesis, thermal stability of bare CNF support, CNF-Pt, CNF-Pd and CNF-Ru catalysts under WAO reaction conditions (i.e. resistance of CNF to air oxidation), was evaluated in a trickle-bed reactor at different reaction temperatures (from 100 to 240 °C) under oxidizing conditions ($p(O_2)$ = 10.0 bar) and feeding the unit with distilled water as a liquid-phase (i.e. absence of reactants). Analysis of liquid-phase samples by TOC and off-gas stream by selective detectors (i.e. CO, CO_2) at any time on stream revealed gasification of the CNF support (formation of CO_2) at the employed oxidative treatment and appearance of organic carbon in the aqueous phase (Fig. 7). The results in Fig. 7a shown for bare CNF confirm that oxidation of carbon to CO_2 starts at temperatures higher than 180 °C (~0.1 vol.% CO_2 at T = 220 °C). The maximum carbon gasification rate may depend on the concentration of surface defects and/or the presence of metal particles in/on carbon nanotubes [11]. The presence of organic carbon in aqueous-phase samples collected in the reactor outlet confirms that oxidative decomposition of the CNF support leading to the formation of unidentified organic intermediates occurs at T = 100 °C and above (Fig. 7a). The same is true for CNF-supported monometallic catalysts (Fig. 7b–d). A comparison of CO_2 concentration profiles obtained over the bare CNF support (Fig. 7a) and catalysts (Fig. 7b–d) shows that the CNF support was more easily oxidized in the presence of supported Pt, Pd and Ru metallic particles (~0.4, 0.3, 1.1 vol.% CO_2, respectively, at 220 °C). For illustration, occurrence of CO_2 in the off-gas stream was in the presence of CNF-Ru catalyst observed already at 100 °C. On the basis of weight measurements, the following sequence of thermal stability under WAO conditions has been observed: CNF (443 mg) > CNF-Pd (270 mg) > CNF-Pt (186 mg) > CNF-Ru (75 mg); the cited numbers represent an amount of catalyst remained after exposing 500 mg of a sample to oxidative treatment (Fig. 7).

Purification of CNT/CNF by various reagents that possess different degrees of oxidation power (i.e. HNO_3, HNO_3/H_2SO_4) affects chemical functionalities on the surface of CNT/CNF, changes the reactivity of these materials and modifies their wetting characteristics [18,19,25,26]. It is reported by Yang et al. [24] who studied oxidation of aqueous phenol solution on HCl-treated and HNO_3/H_2SO_4-treated multi-walled carbon nanotubes using a batch reactor that oxygen-containing functional groups created on the CNT surface during the oxidative treatment, are responsible for the enhanced activity of CNT in the wet-air oxidation of phenol. Additionally, they observed that functionalized CNT exhibits sufficient stability in the oxidation reaction. Introduction of oxygenated groups on the CNT surface is reported to contribute to passivation of the tube surface towards air oxidation [27]. Although HF-treated CNF-based samples were investigated in this

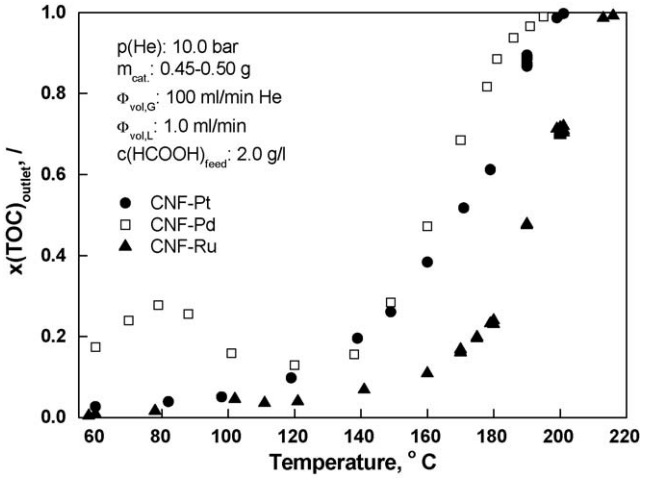

Fig. 8. TOC conversion as a function of temperature measured during the treatment of formic acid in inert He atmosphere over various CNF-supported catalysts. p(He): 10.0 bar, $\Phi_{vol.,L}$: 1.0 ml/min, c(HCOOH)$_{feed}$: 2.0 g/l.

study that might be less stable in oxidative reaction conditions, it is believed that enhanced gasification of the CNF support could be attributed to the fact that due to low volumetric flow rate of the liquid-phase, the external surface of catalyst particles was only partially wetted and thus directly exposed to oxygen in the gas stream. Based on the above results, one can tentatively conclude that HF-treated CNF-based noble metal catalysts, due to insufficient resistance to gasification, might not be suitable solids to carry out liquid-phase oxidation reactions in reactor configurations, where it is rather difficult to achieve complete wetting of the catalyst surface. To clarify this issue, further work is needed by using various kinds of carbon nanofibers (i.e. with different degree of functionalization, purity and/or orientation of graphitic platelets) and continuous-flow reactor systems that favor CNF wetting (e.g. bubble-column fixed-bed reactor). It is believed that the extent of CNF wetting could be further improved by using hydrophilic CNFs (e.g. functionalized with oxygen groups).

3.2.2. Thermal decomposition of formic acid

Experiments performed over bare CNF support at p(He) = 10.0 bar and liquid flow rate of 1.0 ml/min in the temperature range from 60 to 220 °C revealed that CNF support does not exhibit any activity for thermal degradation of formic acid. This is in agreement with the results of our previous study [20], in which it was observed that TiO_2 as a catalyst carrier exhibits no activity for thermal decarboxylation of this compound.

Fig. 8 illustrates TOC conversion as a function of reaction temperature measured during the treatment of aqueous formic acid solution (2.0 g/l) in inert He atmosphere over CNF-Pt, CNF-Pd and CNF-Ru catalysts. It is evident that thermal liquid-phase decarboxylation of formic acid to H_2 and CO_2 starts close to 80 °C and increases with temperature. In the case of CNF-Pd sample, peculiar variation of TOC conversion at temperatures ≤100 °C can be attributed to the decomposition of Pd hydride phase formed at lower temperatures (see Fig. 4). Although among tested materials the CNF-Pd catalyst exhibits the lowest dispersion of surface species (Table 1), 45% TOC conversion of formic acid was achieved at 160 °C over this solid, while the temperature required to reach the same conversion level was increased to 170 and 190 °C in the presence of CNF-Pt and CNF-Ru catalysts, respectively (Fig. 8). This behavior is more clearly seen in Fig. 9, where the TOC conversion as a function of time on stream at a fixed reaction temperature is shown for various catalyst samples. Within an experimental error, constant TOC conversion as a function of time on stream (~91, 88 and 70% at

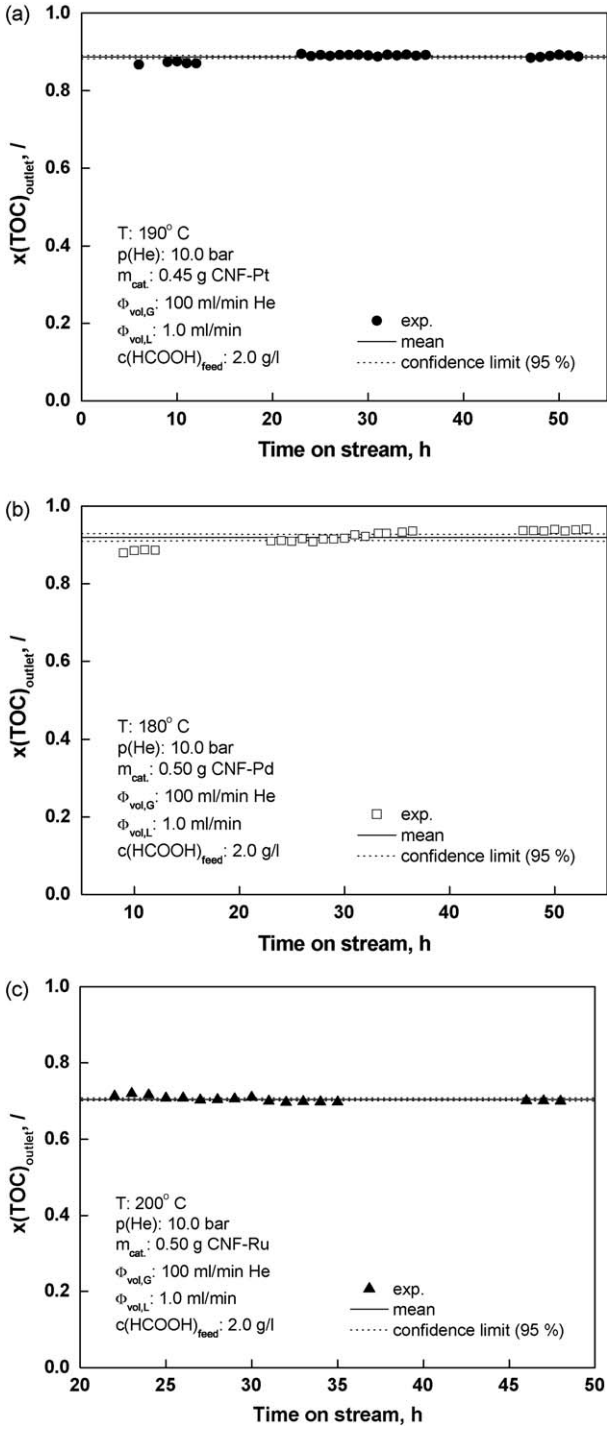

Fig. 9. TOC conversion as a function of time on stream measured over: (a) CNF-Pt, (b) CNF-Pd and (c) CNF-Ru.

T = 180, 190 and 200 °C for CNF-Pd, CNF-Pt and CNF-Ru, respectively) was obtained in the period of 50 h (Fig. 9a–c). On the contrary to CWAO runs (Fig. 5), under the conditions of HCOOH decomposition tests the activity of examined catalysts remains stable. In experiments presented in Figs. 8 and 9, no carbon monoxide was detected in the off-gas stream; carbon dioxide was found to be the only C-containing gaseous product. This confirms that at the employed operating conditions formic acid is thermally decomposed to H_2 and CO_2 over examined CNF-supported catalysts. In terms of TOC conversion, the prepared catalysts exhibit good performance with relation to those reported in the literature [20].

Our previous examination has shown that titania-supported Ru catalysts are active for thermal degradation of formic acid in the temperature range of 60–140 °C and p(He) = 10.0 bar. The most active CNF-Pd catalyst (Fig. 8) and Ru(1.5 wt.%)/TiO_2 catalyst [20] exhibit comparable activities for H_2 formation by thermal decomposition of formic acid under inert He atmosphere. Considering the dispersion of active species equal to 6.1% (CNF-Pd) and 8.6% (Ru/TiO_2), the following activities for liquid-phase decarboxylation of formic acid are derived at T = 140 °C: 1.4 $mol_{HCOOH}/mol_{met}/min$ (CNF-Pd) and 1.1 $mol_{HCOOH}/mol_{met}/min$ (Ru/TiO_2).

3.2.2.1. Spent catalysts. After tests of liquid-phase HCOOH decarboxylation illustrated in Fig. 9, structural and textural characteristics, surface morphology and metal dispersion of spent catalysts (washed with distilled water and dried) were measured. X-ray diffraction of spent catalysts (CNF-Pt-FA, CNF-Pd-FA and CNF-Ru-FA) showed no change in the diffraction peaks associated with the support (Fig. 1b). A comparison of XRD patterns of spent catalysts to those of fresh catalysts indicates that larger metallic particles are created during the treatment of formic acid in inert He atmosphere over the CNF-Pd catalyst (Fig. 1). It is clear that the CNF-Pd-FA pattern shows characteristic diffraction peaks at 40.1, 46.6, 68.1, 82.1 and 86.6° 2θ, which correspond to (1 1 1), (2 0 0), (2 2 0), (3 1 1) and (2 2 2) reflections of crystalline Pd^0 phase (PDF 046-1043). The XRD patterns of spent CNF-Pt-FA and CNF-Ru-FA catalysts only showed diffraction peaks attributed to the CNF support. Metal dispersion in spent catalysts was found to be different to values reported in Table 1, which indicates that in the applied range of operating conditions sintering of Pd as well as Ru particles occurs to a considerable extent (Table 2). This is particularly evident in the case of CNF-Pd catalyst. The Pt dispersion showed little difference after the completion of reaction, which means that among solids tested, the CNF-Pt sample exhibits the best sintering resistance of metal particles (i.e. strong metal–support interaction). Since no catalyst deactivation was observed in the early stage of long-term experiments of liquid-phase HCOOH decarboxylation (Fig. 9), it can be concluded that agglomeration of metallic clusters on the catalyst surface (Table 2) took place when the same samples were precedingly exposed to the highest applied temperatures ($T \geq 200$ °C) in runs depicted in Fig. 8. The SEM analysis (not shown) confirms that the morphology of spent catalysts is similar to that of fresh catalysts (Fig. 2b–d). Furthermore, textural data indicate no significant differences between the total surface area, total pore volume and average pore width in the fresh and spent catalysts (compare Tables 1 and 2). On the contrary to CWAO runs, no weight loss of examined catalyst samples was observed during the thermal liquid-phase decarboxylation of formic acid. These findings confirm that catalysts supported on carbon nanofibers can be efficiently employed to promote liquid-phase reactions in inert/reductive atmosphere.

4. Conclusions

In the present work, carbon nanofibers were prepared by CVD method using γ-alumina-supported iron as catalyst and acetylene as carbon source. Using incipient-wetness impregnation, CNF-supported Pt, Pd, Ru monometallic (2.0 wt.%) catalysts were synthesized with an average particle size of 4, 18 and 20 nm, respectively. BET surface area, total pore volume and average pore diameter of catalysts indicate that deposition of metal did not significantly change the textural properties of the CNF support. The results of H_2-TPR/MS analysis of the CNF and catalyst precursors revealed that reduced Pt and Ru species catalyze reaction between the CNF support and hydrogen ($T \sim 350$ °C) that results in the formation of methane. During WAO runs carried out in the trickle-bed reactor (100–240 °C, $p(O_2)$ = 10.0 bar), the CNF support partially oxidizes and decomposes to CO_2 and unidentified organic intermediates. The following sequence of thermal stability under WAO conditions was observed: CNF > CNF-Pd > CNF-Pt > CNF-Ru.

The CNF support and CNF-Pt catalyst are active in TOC removal during the CWAO of phenol at conditions of $T \geq 180$ °C and 10.0 bar of oxygen. Activity measurements coupled with the physicochemical characterization of spent CNF support and CNF-Pt catalyst after CWAO of phenol demonstrate that higher reaction temperatures are favorable for the oxidation of phenol ($T \geq 200$ °C). As HF-treated CNF-based catalysts are prone to gasification in the CWAO process, further work is needed to develop and test materials with appropriate surface properties.

The CNF support is not active in TOC removal during thermal decarboxylation of formic acid at conditions of T = 60–220 °C. CNF-supported monometallic catalysts enhance thermally induced liquid-phase decarboxylation of formic acid to H_2 and CO_2 at $T \geq 80$ °C. Constant and high TOC conversion as a function of time on stream (~91, 88 and 70% at T = 180, 190 and 200 °C for CNF-Pd, CNF-Pt and CNF-Ru, respectively) was obtained in the period of 50 h. The most active CNF-Pd catalyst and conventional Ru/TiO_2 catalysts exhibited comparable activities for H_2 formation by thermal decomposition of formic acid under helium atmosphere. The results of catalytic tests and physicochemical characterization of used catalysts after treatment of aqueous formic acid solutions confirm that catalysts supported on carbon nanofibers can be efficiently used to promote liquid-phase reactions in inert/reductive atmosphere.

Acknowledgement

The authors gratefully acknowledge the financial support of the Ministry of Education, Science and Technology of the Republic of Slovenia through Research program no. P2-0152.

References

[1] F. Luck, Catal. Today 53 (1999) 81.
[2] A. Cybulski, Ind. Eng. Chem. Res. 46 (2007) 4007.
[3] L. Oliviero, J. Barbier Jr., D. Duprez, A. Guerrero-Ruiz, B. Bachiller-Baeza, I. Rodriguez-Ramos, Appl. Catal., B 25 (2000) 267.
[4] T. Cordero, J. Rodríguez-Mirasol, J. Bedia, S. Gomis, P. Yustos, F. García-Ochoa, A. Santos, Appl. Catal., B 81 (2008) 122.
[5] F. Stüber, J. Font, A. Fortuny, C. Bengoa, A. Eftaxias, A. Fabregat, Topics Catal. 33 (2005) 3.
[6] S. Iijima, Nature 354 (1991) 56.
[7] P.M. Ajayan, S. Iijima, Nature 361 (1993) 333.
[8] T.W. Ebbesen, H.J. Lezec, H. Hiura, J.W. Bennett, H.F. Ghaemi, T. Thio, Nature 382 (1996) 54.
[9] H. Dai, J.H. Hafner, A.G. Rinzler, D.T. Colbert, R. Smalley, Nature 384 (1996) 147.
[10] P.M. Ajayan, Chem. Rev. 99 (1999) 1787.
[11] P. Serp, M. Corrias, P. Kalck, Appl. Catal., A 253 (2003) 337.
[12] Z. Liu, X. Lin, J.Y. Lee, W. Zhang, M. Han, L.M. Gan, Langmuir 18 (2002) 4054.
[13] C. Wang, M. Waje, X. Wang, J.M. Tang, R.C. Haddon, Y.S. Yan, Nano Lett. 4 (2004) 345.
[14] J.M. Planeix, N. Coustel, B. Coq, V. Brotons, P.S. Kumbhar, R. Dutartre, P. Geneste, P. Bernier, P.M. Ajayan, J. Am. Chem. Soc. 116 (1994) 7935.
[15] J.P. Tessonnier, L. Pesant, G. Ehret, M.J. Ledoux, C. Pham-Huu, Appl. Catal., A 288 (2005) 203.
[16] J. García, H.T. Gomes, P. Serp, P. Kalck, J.L. Figueiredo, J.L. Faria, Catal. Today 102–103 (2005) 101.
[17] H.T. Gomes, P.V. Samant, P. Serp, P. Kalck, J.L. Figueiredo, J.L. Faria, Appl. Catal., B 54 (2004) 175.
[18] G. Ovejero, J.L. Sotelo, M.D. Romero, A. Rodríguez, M.A. Ocaña, G. Rodríguez, J. García, Ind. Eng. Chem. Res. 45 (2006) 2206.
[19] J. García, H.T. Gomes, P. Serp, P. Kalck, J.L. Figueiredo, J.L. Faria, Carbon 44 (2006) 2384.
[20] A. Pintar, J. Batista, T. Tišler, Appl. Catal., B 84 (2008) 30.
[21] D.M. Ruthven, Principles of Adsorption and Adsorption Processes, John Wiley and Sons, New York, 1984.
[22] C. Amorim, G. Yuan, P.M. Patterson, M.A. Keane, J. Catal. 234 (2005) 268.
[23] A. Pintar, J. Batista, J. Hazard. Mater. 149 (2007) 387.
[24] S. Yang, X. Li, W. Zhu, J. Wang, C. Descorme, Carbon 46 (2008) 445.
[25] C.-H. Li, K.-F. Yao, J. Liang, Carbon 41 (2003) 858.
[26] V. Datsyuk, M. Kalyva, K. Papagelis, J. Parthenios, D. Tasis, A. Siokou, I. Kallitsis, C. Galiotis, Carbon 46 (2008) 833.
[27] A. Solhy, B.F. Machado, J. Beausoleil, Y. Kihn, F. Gonçalves, M.F.R. Pereira, J.J.M. Órfão, J.L. Figueiredo, J.L. Faria, P. Serp, Carbon 46 (2008) 1194.